Electrochimica Acta 297 (2019) 916–928

Contents lists available at ScienceDirect

Electrochimica Acta

journal homepage: www.elsevier.com/locate/electacta

A systematic study of kinetics in mesocarbon microbeads anodes in presence of nano-conductive additives

Salahuddin Ahamad, Amit Gupta*

Department of Mechanical Engineering, Indian Institute of Technology Delhi, Hauz Khas, New Delhi, 110016, India

ARTICLE INFO

Article history:
Received 3 August 2018
Received in revised form
15 November 2018
Accepted 1 December 2018
Available online 7 December 2018

Keywords:
Li-ion batteries
MCMB
Nano-fillers
Activation energy
Diffusivity

ABSTRACT

Nano-conductive additives in composite electrodes play a significant role in influencing the electrochemical performance of the carbon anode in Li-ion batteries. These additives with a high electronic conductivity lead to the formation of a uniform solid-electrolyte interfacial layer, improved cycle life, and rate capability. In this work, the parameters that lead to such a performance improvement, namely the kinetic and transport properties, are carefully studied with carbon black (CB), carbon nanotubes (CNT) and a mixture of the two as conductive additives in mesocarbon microbeads (MCMB) anode. Experimental measurements indicate that the electrochemical reaction rate is controlled by interfacial kinetics up to moderately high C-rate (<6C). Though nano-additives do not affect the solid phase diffusivity, the diffusion of Li-ion is considerably influenced by stages and their coexistence that is revealed through X-ray diffraction of cells at different depths of discharge. Using electrochemical impedance spectroscopy of half-cells cycled at different temperatures, the activation energy for charge transfer reaction and activation energy for SEI layer diffusion are estimated. The results exhibit an improvement in electron transfer and an ionically conducting SEI layer with the use of a mixture of CB and CNT as conductive additives. It is expected that the estimated kinetic and transport parameters and their temperature dependence for the additives under consideration will be of tremendous utility in the thermal, electrochemical, or aging modeling of batteries employing MCMB as anode material.

© 2018 Elsevier Ltd. All rights reserved.

1. Introduction

A major hurdle for electric vehicles gaining significant traction in the automotive industry is the high cost of Li-ion batteries. Moreover, the expected increase in demand for electric vehicles makes Li-ion battery technology even more critically desired. Thus, it is imperative to develop next-generation Li-ion batteries capable of providing higher energy and power densities with extended cycle-life [1,2]. Currently, the electrodes chemistries and their electrochemical performances are tested via experiments at various stages starting from battery design, cell assembly, and their cycling in most cases. These methods are known to be slow and expensive in terms of time and resources. Alternatively, a numerical approach using cell-level models to simulate Li-ion battery performance is a relatively cheaper option. However, a physicochemical model based on fundamental governing equations of migration and diffusion processes as well as the kinetics of intercalation will require precisely evaluated model parameters for the material under consideration. Accurately measured kinetics and transport parameters will hold the key to derive reliable conclusions about the internal state of a Li-ion battery.

Commercially, graphite is the choice of the negative electrode in Li-ion battery due to its low cost, low operating potential vs. Li/Li^+, high capacity, good reversibility and structural stability [3,4]. Mesocarbon microbeads (MCMB) is a popular form of graphite owing to its narrow particle size distribution (4–16 μm), higher packing density and large edge plane surface area than graphitic flakes [5–8]. The relatively higher edge plane proportion provides faster electron transfer rates and stronger electrocatalytic activity than those of the basal plane [9,10]. Moreover, incorporating conducting nano-additives in composite electrodes has a significant role in influencing the interfacial charge transfer kinetics of carbon anode in Li-ion batteries [11,12]. A higher electronic conductivity of the composite electrode has been shown to be directly responsible for a uniform distribution of electrons at the surface of active particles resulting in the formation of a uniform active double layer [13]. Various techniques, such as carbon coating [14], graphene wrapping [15,16], lattice doping [17–19] and the addition of

* Corresponding author.
E-mail address: agupta@mech.iitd.ac.in (A. Gupta).

https://doi.org/10.1016/j.electacta.2018.12.006
0013-4686/© 2018 Elsevier Ltd. All rights reserved.

metallic particles (copper and nickel) [20], have been suggested to improve conduction and surface distribution of electrons in the composite electrode. The basic idea behind these improvements has been to reduce the interfacial charge transfer resistance that involves both electrons and Li-ions. In this regard, our earlier work has shown that MCMB electrodes with hybrid conducting additives display a synergistic increase in electrical conductivity, initial capacity, capacity retention and SEI layer stability [21] which has to do with improved interfacial kinetics of Li-ion de-solvation and charge transfer reaction.

Typically, the processes involved during intercalation in Li-ion battery electrodes are: (i) liquid phase diffusion of solvated Li-ion to the surface of active material, (ii) interfacial charge transfer reaction, (iii) solid-state diffusion of lithium, and (iv) crystallographic changes in the structure of active material [22]. Among these processes, charge transfer at electrode/electrolyte interface and Li-ion diffusion in the solid phase of active material are inherently slow processes in contrast to the transport of Li-ion in the solution phase. Moreover, graphitic materials show a considerable variation in their texture and crystal structure during intercalation/deintercalation [21]. To attain a clear understanding of the influence of these changes on Li-ion transport in the solid phase, manifested in terms of changes in voltage profile, becomes critically important. Although graphite has excellent implications for Li-ion batteries, there still prevail uncertainties regarding parameters associated with interfacial kinetics and phase transport. For example, Li-ion diffusivity in solid phase studied by several groups ranges from 10^{-6} to 10^{-16} cm^2/s [23–28]. Moreover, exchange current density as determined by several authors [29–32] is usually not scaled to the actual electrochemical surface area. This makes the use of the reported value for different microstructures infeasible. In addition, parameters such as charge transfer coefficient, the activation energy for desolvation, and the activation energy of diffusion for carbon electrodes in the presence of additives have not received much attention.

Thus, we present a systematically conducted experimental study to (a) gain an insight into the structural transformation of MCMB during intercalation/deintercalation, (b) estimation of transport parameters, and (c) investigate kinetics of electron transfer reaction for MCMB anode in the presence of carbon black, carbon nanotubes and a mixture of the two as conducting nano-additives. Specifically, quantification of exchange current density, activation energies (for charge transfer, SEI layer migration and solid-state diffusion), and solid-state diffusivity are the focus of this work. A number of complementary electrochemical methods, such as galvanostatic cycling, electrochemical impedance spectroscopy (EIS), galvanostatic intermittent titration technique (GITT), and X-ray diffraction (XRD) to determine structural changes associated with lithiation have been employed to probe intercalation/deintercalation characteristics in MCMB anode. It is envisaged that the estimated kinetic and transport parameters in presence of nano-additives will be of importance to researchers working on developing thermo-electrochemical or aging models of batteries employing MCMB as anode material.

2. Experimental

2.1. Fabrication and characterization of electrode

The composite electrodes were fabricated using commercially available MCMB graphitic powder with different conducting additives CB, CNT, and a mixture of CB and CNT. The active material particles have spherical morphology with size in the range of 2–20 μm. CB, a widely used conducting additive in battery electrodes, has aciniform (grape-like) morphology of fused spherical primary particles that form an aggregate of diameter 20–30 nm (refer to Fig. S1 (a) in Supplementary Information). The carbon nanotubes used in this work were multiwalled (MWCNT) with an average diameter of 10–30 nm (Fig. S1 (b) in Supplementary Information). The structural differences of conductive additives were investigated by XRD and Raman spectroscopy measurements and then verified with HRTEM (the patterns are shown in Fig. S2 of Supplementary Information). The electrodes comprised of 88 wt. % MCMB, 4 wt. % conductive additives (CB, CNT or CB + CNT) and 8 wt. % PVdF (polyvinylidene difluoride) as a binder. The slurry was prepared in NMP solvent and coated onto a battery grade copper foil. The coated films were dried at 120 °C under vacuum overnight. The electrode laminates were calendered to about 12% of initial film thickness to ensure good contact between the electrode components and the current collector. Then, electrode discs with a diameter of 12 mm were punched from the calendered laminate. The thickness of the coated film was typically 35–40 μm with the active mass ca. 3.5 mg. The detailed steps followed to fabricate the electrode laminate are described in our earlier work [21].

The morphologies and microstructure of active material, conductive additives and composite electrode were analyzed using Zeiss EVO 50 Scanning Electron Microscope (SEM) operated at 30.0 kV and high-resolution transmission electron microscope (HRTEM; Tecnai TF20, FEI, USA) operated at 200 kV. X-ray diffraction (XRD) pattern was conducted on a Rigaku D/max-2500VB system (Rigaku Co., Tokyo, Japan) using Cu/K_α radiation ($\lambda = 1.5406$ Å). BET analysis of MCMB was also carried out to estimate the gravimetric surface area using Gemini 2360 Surface Area Analyser.

2.2. Cell fabrication and electrochemical testing

Two-electrode CR2016 coin type half-cells were assembled in a vacuum glove box (Jacomex SAS, France) with both moisture and oxygen level below 0.5 ppm. A porous 25 μm thick polypropylene film as a separator and 1 M $LiPF_6$ solution in a mixture of ethylene carbonate (EC) and dimethyl carbonate (DMC) mixed in a 1:1 vol ratio (Sigma-Aldrich) was used as the electrolyte. A Li-metal foil with 16 mm diameter and 400 μm thickness was used as counter and a reference electrode. Finally, the cells were sealed by electric coin cell crimping machine (MTI-Corp., CA, USA).

Electrochemical characterization was carried out by conducting cyclic voltammetry (CV) in the voltage range of 0.0–2.0 V at a scan rate of 0.01 mV s^{-1} using Biologic VMP3 testing workstation (refer to Fig. S4 of Supplementary Information). The rate capability of electrodes with different conducting additives was studied by charge-discharge cycling at 1C and 4C-rates with lower and upper cutoff potentials of 0.005 V and 2.0 V vs. Li/Li^+, respectively (representative results are shown in Fig. S5 of Supplementary Information). Electrochemical impedance spectroscopy (EIS) measurements were performed in the frequency range 5 mHz–200 kHz with an applied bias voltage of 5 mV between the counter and working electrodes.

To conduct a thermal study, a temperature-controlled chamber as shown in Fig. 1 was designed and fabricated to carry out experiments with reproducible EIS results in a wide temperature range. The chamber was equipped with PID temperature controller with an accuracy of ±0.01 K, K-type thermocouple, and 500 W heating jacket wrapped around 12 cm diameter glass cylinder. The thermocouple probe was placed at the center and the cell holder close to the probe. A thermometer was situated right on the top of the cell to monitor the temperature from outside. The assembly was covered by fire resistance asbestos cloth and assembled in an enclosure as shown in Fig. 1 to minimize the loss of heat from the chamber.

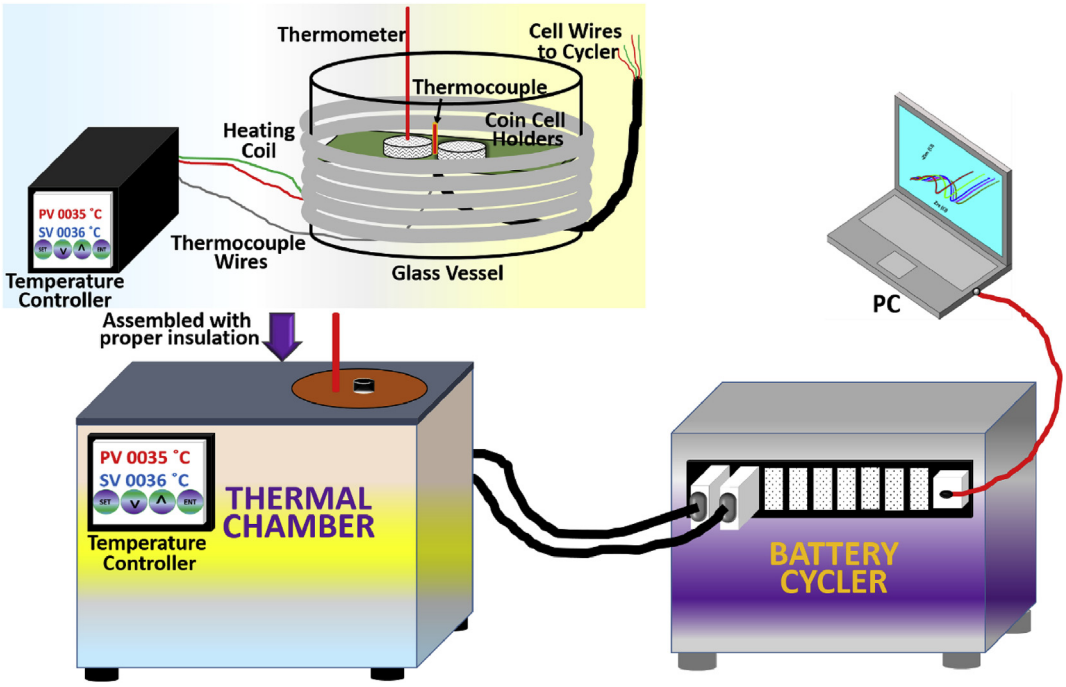

Fig. 1. Schematic of a thermal chamber designed for temperature variation study in Li-ion coin cells.

3. Results and discussion

3.1. Electrochemically active surface area

Graphite has two kinds of planar areas: basal and edge. It is well known that the electrochemical reaction occurs only on the edge plane (also referred to as the electrochemical active surface area, S_{ECAS}) [33–35]. As the electron transfer rates on graphite edge-planes are ca. 105 times higher than graphite basal-plane [36]. This has been attributed to the localization of high energy electrons on these edge surfaces. In literature, the exchange current density and solid phase effective diffusivity are either not scaled to the actual electrochemically active interfacial area [29] or evaluated based on the geometric area [37]. The geometric area could be a good approximation for the actual interfacial surface area in case of ultrathin film electrode [37], but it cannot be used for thin film electrodes. Clearly identifying the area of electrochemically active surfaces is critically important as it eliminates the variability in any parameter value related to electrodes under examination due to variations in geometric area and mass of active material [38].

The active material (source: TOB New Energy, China) had a size distribution between 4 and 18 μm with D_{50} of 10.12 μm and was used as received. Fig. 2(a)-(b) shows the SEM image of MCMB particles and a magnified image of a single particle, respectively, to illustrate the surface texture of the active material. The particle size distribution (PSD) histogram of MCMB particles based on the observation of over 200 particles is illustrated in Fig. 2(c) with a well fitted normal distribution curve. The descriptors of particle size derived from the data are also presented in the inset of Fig. 2(c). The electrochemical active surface area was estimated by using image processing of the SEM micrographs of MCMB particles by repeating it for five different samples (each basis comprising of approximately 50 particles). A schematic illustration of edge and basal planes of graphitic crystallite is presented in Fig. 2(d). Also, MCMB used in this work is a soft carbon graphitized at high temperature (~2500 °C) in which the crystallite are aligned and the value of their structural parameters such as d_{002}, L_c and L_a are 0.3354 nm, 11.5 nm and 37.2 nm, respectively, as evaluated through XRD analysis.

The average particle size D_{avg} has been calculated using the equation, $D_{avg} = \sum n_i D_i / \sum n_i$, where D_i is the diameter and n_i is the number density. The corresponding active specific surface area or electrochemically active surface (ECAS) for MCMB particles, S_{ECAS} (m^2/g), can be approximated using the following equation [39]:

$$S_{ECAS} = \frac{6}{\rho}\left(\frac{\sum n_i D_i^2}{\sum n_i D_i^3}\right) \quad (1)$$

where ρ (2.23 g/m^3) is the density of MCMB. The MCMB average diameter is 10.17 μm as observed in Fig. 2(c) and electrochemically active surface area evaluated in terms of unit mass was 2326 cm^2/g. As graphite has a porous structure, some of the micro-pores (pore size < 2 nm) are also N_2-accessible. However, these micro-pores are not electrolyte accessible due to the larger size of the solvation sheath (solvated Li-ion) in comparison to N_2 molecule [40]. Using evidence from Table 1, we neglect the contribution of these micro-pores to the electrochemical performance and consider the specific edge area as the actual active interface area in this study. Therefore, the surface area with edge-plane was considered to be a true reflection of the area of MCMB electrode. Further, the calculated value of SECAS is in good agreement with the theoretical value of 2617 cm^2/g reported elsewhere [38]. Since the surface area predicted by BET was not of the same order as that found using image processing and in the literature [38], further analysis using BET was not pursued.

3.2. Kinetics at the solid-electrolyte interface

For standard graphitic electrodes, the limiting current for charging (lithiation) and discharging (delithiation) have been reported to be ~2C and ~20C, respectively [41]. Therefore, we probe the performance under discharging mode to study the kinetics and

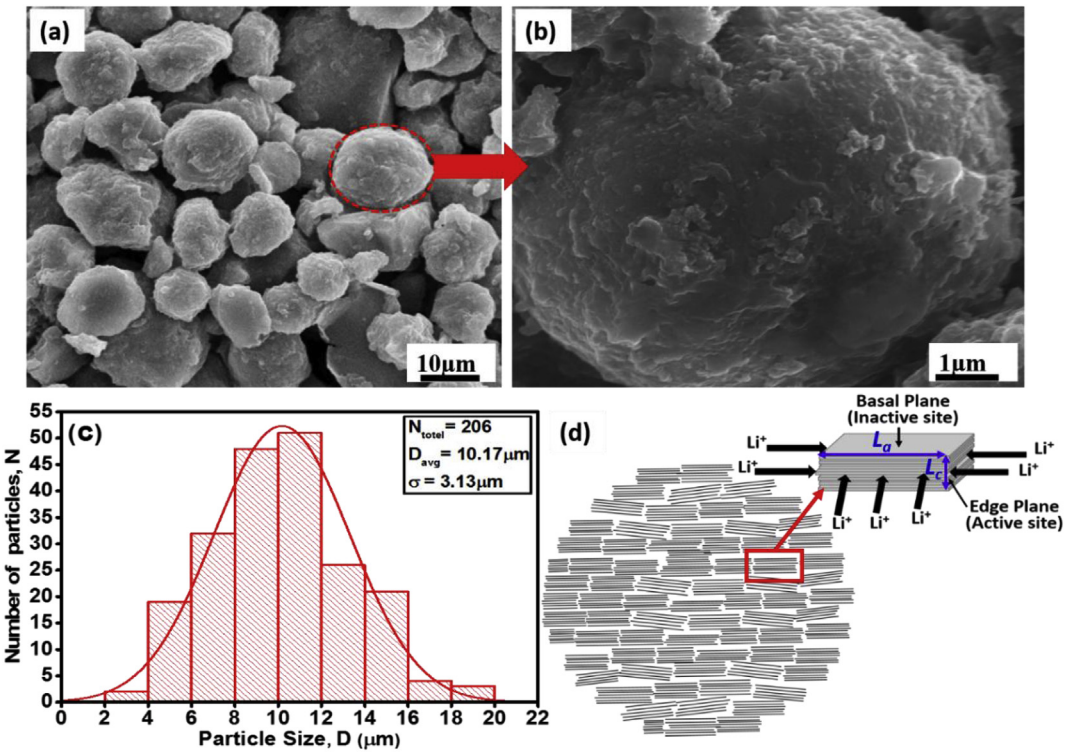

Fig. 2. (a) SEM image of MCMB particles, (b) SEM image of a single particle to demonstrate edges, (c) corresponding particle size distribution histograms measured from image processing, and (d) schematic of MCMB sphere and a graphite crystallite to illustrate the reaction sites.

Table 1
Particle size and specific surface area of MCMB carbon.

Sample	D_{10} (μm)	D_{90}(μm)	D_{avg}(μm)	S_{BET} (m^2/g)	S_{ECAS} (m^2/g)
MCMB	5.98	14.42	10.17	1.37	0.2326

transport in the presence of conducting additives for a wide current range. The cells were charged at galvanostatic mode at 1C-rate between the cut-off voltages (2.0 V–0.005 V vs. Li/Li^+) followed by potentiostatic mode at 0.005 V until current dropped to C/20 prior to each measurement of the discharge profile.

The reaction rate is apparently controlled by the interfacial electrochemical reaction, solid-state diffusion of Li-ion and crystallographic structural changes in the active material during the lithiation and delithiation processes. To demonstrate these facts, the galvanostatic discharge curves at various currents for MCMB electrodes with 4% by weight of CNT as conducting additives as well as the comparison of discharge voltage profiles at different currents for the electrodes having CB, CNT and hybrid CB-CNT conducting nano-fillers are shown in Fig. 3(a) and (b) respectively. It can be seen from Fig. 3(a) that at 6C current the electrode exhibits almost 92% of discharge capacity obtained at C/5 rate, with overpotential successively increasing with increase in magnitude of cycling current. It may be inferred from Fig. 3(a) that mass-transport limitations are not so dominant until 6C discharge rate. In other words, we expect a small Li-ion concentration gradient inside the MCMB electrode and the reaction rate is controlled by the interfacial charge transfer reaction. In contrast, the discharge curve displays a narrow voltage plateau at discharge rates more than 6C and consequently shows a lower discharge capacity. Clearly, a high Li-ion concentration gradient is developed inside MCMB particles with the electrode potential rising rapidly to the cut-off value with Li-ions depleted at the surface while substantial amount remains towards the center of the particle that is unutilized. Thus, at higher discharge current the electrochemical reaction rate is controlled by solid-state diffusion [42]. Moreover, it can also be observed from Fig. 3(b) that the electrodes with hybrid conducting additives display an extended voltage plateau. In case of electrodes having only CB as nano-fillers, the potential plateau shows significant deviation in comparison to the electrodes with only CNT or hybrid CB-CNT nano-fillers. As shown in Fig. 3(b), the polarization becomes increasingly larger with increasing C-rate. The large polarization with CB suggests a relatively poor transport of electrons through conduction which is due to point contact. On the other hand, the electrodes containing CNT and hybrid CB-CNT exhibit low polarization due to the formation of well-connected MCMB-CB-CNT chains resulting in improved electrochemical kinetics as well.

This behavior can also be understood in terms of a Tafel plot where kinetic overpotential (η_k) vs. current ln(i_k) is plotted at different depths of discharge (DOD). The relation between current and the electrode potential for the electrochemical reaction $Li^+ + e^- \rightleftarrows Li$ can be described by phenomenological Butler-Volmer kinetics [43],

$$i_k = i_0\left[\exp\left(\frac{\alpha ne}{k_B T}\eta_k\right) - \exp\left(-\frac{(1-\alpha)ne}{k_B T}\eta_k\right)\right] \quad (2)$$

where $i_k$is the current density, i_0 is the exchange current density, $\alpha$is the symmetry factor, $\eta_k$is the kinetic overpotential, $e$is the elementary electronic charge, n is the number of electrons involved in the electrochemical reaction, k_B is the Boltzmann's constant and T is the absolute temperature.

Butler-Volmer and Tafel analysis are based on macroscopic concepts with the rate of the reaction expressed in terms of phenomenological parameters, k and α. Alternative approaches such as Marcus-Hush (MH), Marcus-Hush-Chidsey (MHC) etc.

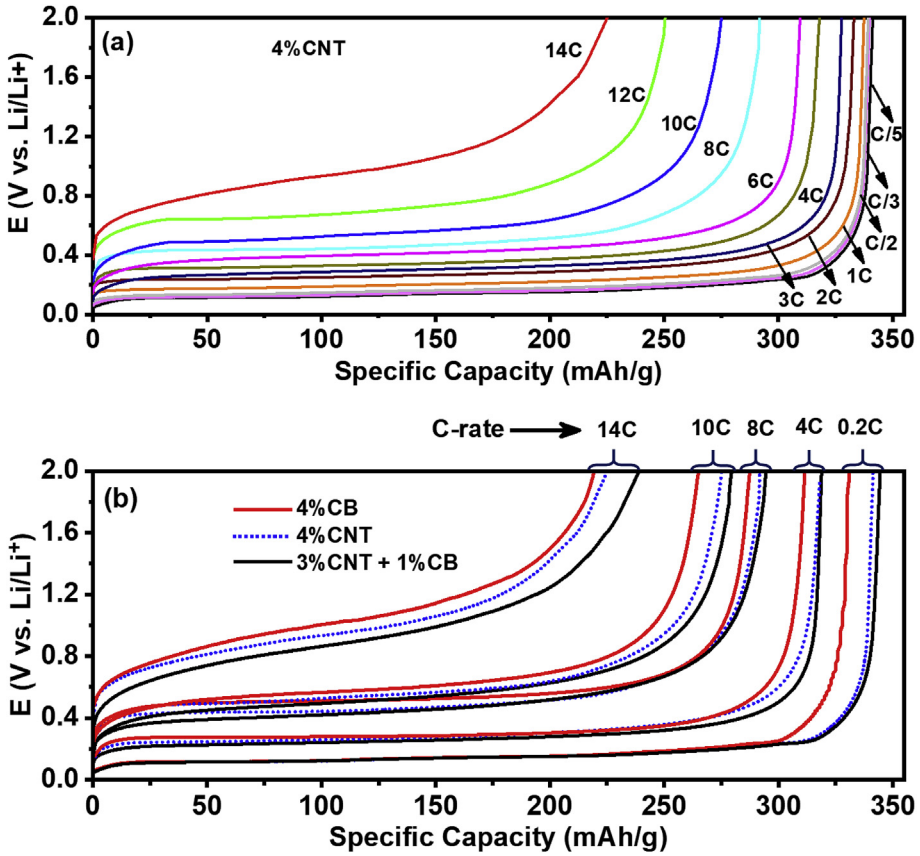

Fig. 3. (a) Galvanostatic discharge curves of MCMB electrode composed of CNT as additives measured between 0.005 V and 2.0 V at 25 °C at various currents. Lithiation of the electrode before every discharge was done at 1C-rate to 0.005 V vs. Li/Li^+ followed by constant voltage charging at 0.005 V till current dropped to C/20. (b) Discharge profiles of various electrodes with different conducting additives compared at various C-rates.

[44,45] can also provide insight into the kinetics using microscopic behavior; though in terms of representation of kinetics, the difference between the two approaches is not significant (especially in case of Li-ion battery with liquid electrolyte) [46]. Since the former is easier to implement and evaluate, most models of kinetics assume Butler-Volmer kinetics as applicable to real electrodes.

In this work, the inherent kinetics in the active material has been evaluated using thin film (~30 μm) as the model electrode [47–49]. There are many factors that make parameter estimation in a thick electrode difficult and prone to errors. These are, (a) the mass transport limitations of lithium ions in the electrolyte phase as well as the impedance against movement of electrons in the solid phase of the electrode becoming dominant, (b) non-uniform variation of potential and current density in thick electrodes leading to spatially varying kinetics, (c) poor heat dissipation in case of thick electrode causing non-uniform temperature distribution further exacerbating the assumption of uniform kinetics, and (d) ionic current density through the separator increases which causes higher overpotential, potentially leading to lithium plating on graphite particles in vicinity to the separator during charging. In addition to this, the SEI formed on the surface of active material also has an indirect influence on the electrochemical performance. The composition and thickness of SEI formed vary within the electrode. A thicker electrode will correspondingly have a higher current density for the same form factor cell. This fact coupled with high Li-ion concentration in the electrolyte results in rapid SEI growth near the separator, while the same is not expected to be true for other sites in the electrode where the current density diminishes due to mass transfer limitations. Due to these limitations of thick electrodes, kinetic measurements were only performed with thin electrodes in this work.

As mentioned in section 3.1, each discharge current was normalized by the electrochemically active surface area (S_{ECAS}) in our experiments. The magnitude of the kinetic overpotential for an electrode at potential Ucan be written as$\eta_k = |U - U_{OCP}|$, where U_{OCP} is open circuit potential [42]. For an accurate measurement of kinetic overpotential, the voltage drop due to cell internal resistance i.e. the effect of iR loss cannot be ignored. However, the internal resistance of cell increases considerably with the increasing number of cycles. As shown in Fig. 4(a) and (b), the internal resistance can be captured by recording EIS spectra after a fixed number of cycles. The increase in internal resistance is believed to be due to thickening of SEI layer during cycling, binder decomposition that leads to loss of contact of the active material with conducting fillers and the current collector, oxidation of conducting nano-fillers and corrosion of current collector foil. As a result, $\eta_k$for carbon anode in Li-ion cell under discharging mode is defined as $\eta_k = (U - U_{OCP} - iR_{int})$.

At moderately high discharge current or when kinetic overpotential, $\eta_k > 118$mV[42], the forward reaction, i.e., anodic reaction rate dominates the cathodic reaction rate and the latter can be ignored. In other words, the electrochemical reaction kinetics can be assumed to be in the Tafel zone and equation (2) reduces to

$$\eta_k = \left(\frac{2.303k_BT}{\alpha ne}\right)\log i_k - \left(\frac{2.303k_BT}{\alpha ne}\right)\log i_0 \quad (3)$$

Thus, the exchange current density i_0 with different conducting

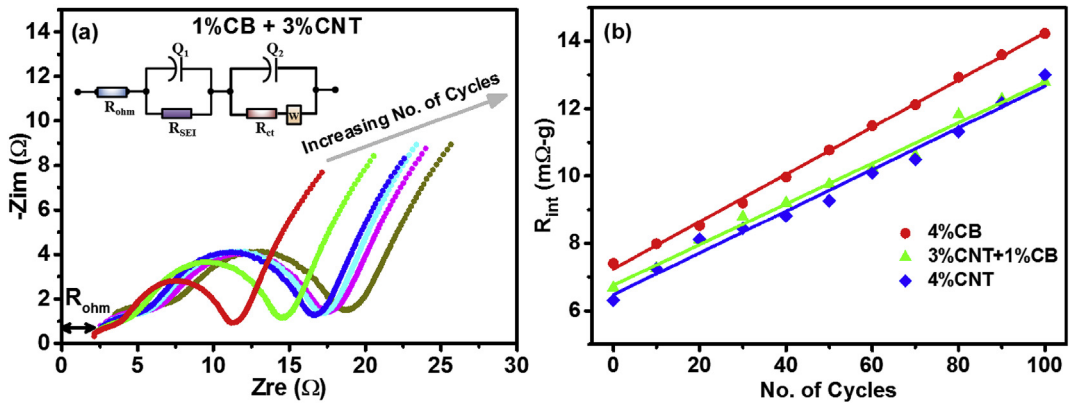

Fig. 4. Effect of cycling on internal resistance, R_{int}. (a) EIS spectra recorded after the cell was charged/discharged for 10 cycles at 1C-rate. (b) The plot of internal resistance vs. cycle number.

additives has been obtained from the linear part of η_k vs. $\log i_k$ plot (i.e., Tafel plot).

The Tafel zone for the electrodes containing different nano-fillers between 10% and 90% DOD was probed further for currents up to 10C. For illustration, the Tafel plot for electrodes containing CB, CNT, and CB + CNT conducting nano-fillers at 20% of DOD are shown in Fig. 5(b), c, and d, respectively. The figures are demarcated into three different regimes. A quasi-equilibrium zone can be seen in the voltage range of 30–80 mV at slow discharge rates (<1C-rate) that suggests that the reaction rate is controlled by the interfacial charge transfer reaction. This is followed by a linear Tafel zone at a moderately high discharge current (2C to 6C-rate) for which the kinetic overpotential lies in the range of 120–270 mV and indicates that the reaction rate is still kinetically controlled and is irreversible. For currents higher than 10C, the Tafel plot deviates from linearity due to mass transfer limitations. This region is demarcated as the mass transfer limited zone. According to equation (3), the exchange current density can be determined from the intercept at zero kinetic overpotential. The exchange current density values hence obtained at the different depth of discharge (DOD) are given in Table 2.

A careful examination of values listed in Table 2 reveals that the composite electrodes with hybrid conducting fillers (1% CB + 3% CNT) possess faster kinetics for delithiation than electrodes containing only CNT or CB as a conductive additive, implying that hybrid conducting fillers provide superior kinetics. This

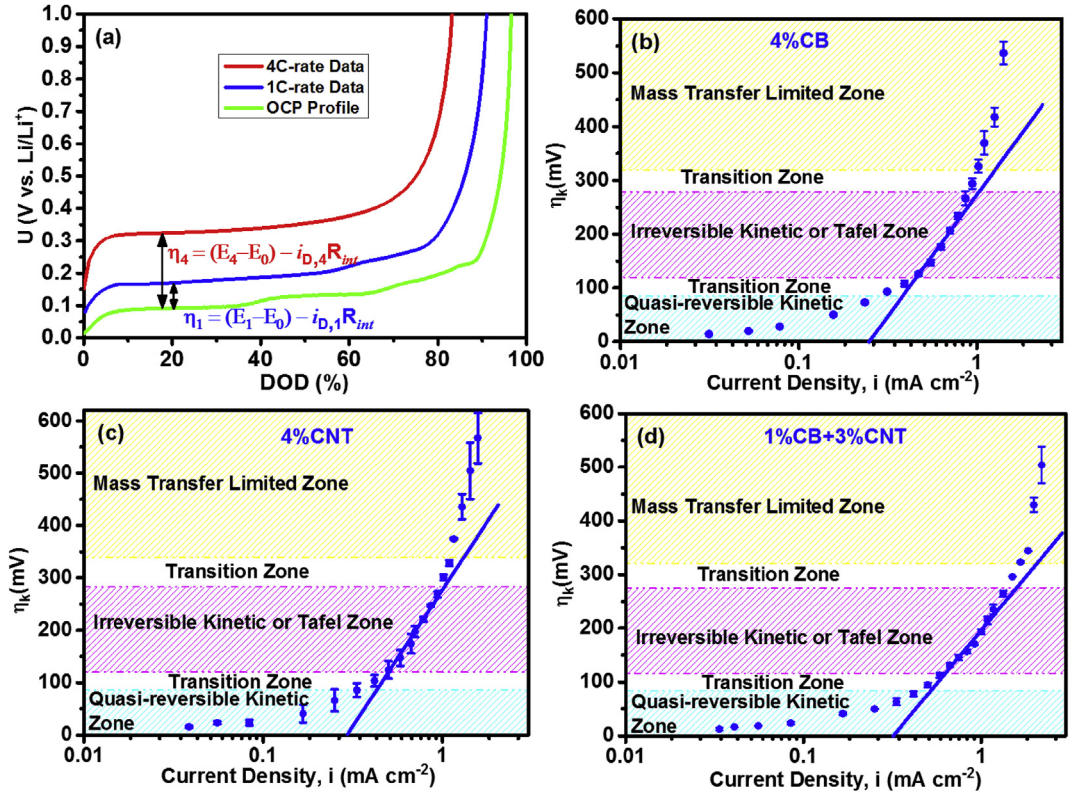

Fig. 5. (a) Schematic representation of the method employed for calculating overpotential from voltage profiles. (b)–(d) Tafel-like plot for MCMB carbon with different conducting additives ((b): 4% CB, (c): 4% CNT, and (d): 1%CB + 3%CNT).

Table 2
Exchange current density (i_0) evaluated at different depth of discharge (DOD) values.

Conducting Fillers	Exchange DOD Current Density	10%	20%	30%	40%	50%	60%	70%	80%	90%
4%CB	$i_0 \times 10^4$(A/cm^2)	2.14	2.40	2.04	2.14	2.17	2.58	2.27	2.69	2.15
4%CNT	$i_0 \times 10^4$(A/cm^2)	2.80	2.90	2.10	2.39	2.50	2.62	2.31	2.74	2.26
1%CB + 3%CNT	$i_0 \times 10^4$(A/cm^2)	2.59	3.20	2.65	2.75	2.85	2.77	2.89	3.16	2.34

quantification of exchange current density offers credence that a conducting scaffold formed by mixing 1% CB and 3% CNT by weight offers short-range and long-range conducting pathways, together with sufficient contact between MCMB particles capable of improving electron and solid-phase lithium transport. It should be noted that the values listed in Table 2 are in reasonable agreement with those reported in earlier studies using EIS technique at 20% DOD for a single MCMB particle electrode (6×10^{-4}A/cm^2 [50], 4.9×10^{-4}A/cm^2 [24]) and for graphitic electrode (0.2×10^{-4}A/cm^2 [51]).

3.3. Thermal dependence of interfacial kinetics

A well-connected network of conducting nano-fillers play an essential role in determining the electrochemical performance of composite electrode in terms of discharge capacity, rate capability and a thin and mechanically stable SEI layer [21]. In the past, some studies dealing with interfacial kinetics in Li-ion battery electrodes and having investigated the effect of electrolytes [52–58], salt in electrolyte [54,58], and influence of edge orientation [59] exist. However, a systematic assessment of the role of different aspect ratio nano-fillers on the composite electrode performance in terms of evaluation of the interfacial kinetics is still missing. Therefore, we examine the thermal dependence of interfacial kinetics of MCMB electrodes with different conductive additives (CNT and CB individually and CNT-CB as a hybrid filler) in this section.

Fig. 6(a) shows the typical Nyquist plots of MCMB electrode at various temperatures with 1%CB and 3% CNT by weight as conducting fillers. It should be noted that the impedance values have been normalized with respect to the electrochemically active surface of the active material for the sake of meaningful comparison of the EIS curves (and due to slight variation in overall weight between different electrodes prepared in this work). Prior to conducting EIS, the test cell surface-chemistry was stabilized by performing constant current cycling between 2 V and 0.005 V vs. Li/Li$^+$ at 0.2C-rate for five cycles. Afterward, the cell potential was stabilized at 0.16 V vs. Li/Li$^+$ until the residual current density fell under 0.08 mAcm^{-2} to ensure the reproducibility of EIS spectra and their deconvolution. In other words, it was observed that the depressed semicircles of recorded EIS spectra for graphitic electrode are well defined at the potential of reversible Li-ion intercalation/deintercalation. Consequently, the impedance data collected would seemingly reflect interfacial properties. The impedance measurements were performed in the frequency range of 5 mHz–200 kHz, and a bias voltage of 5 mV AC amplitude against open circuit potential between the counter and working electrodes was applied. Before conducting impedance measurements, the cell

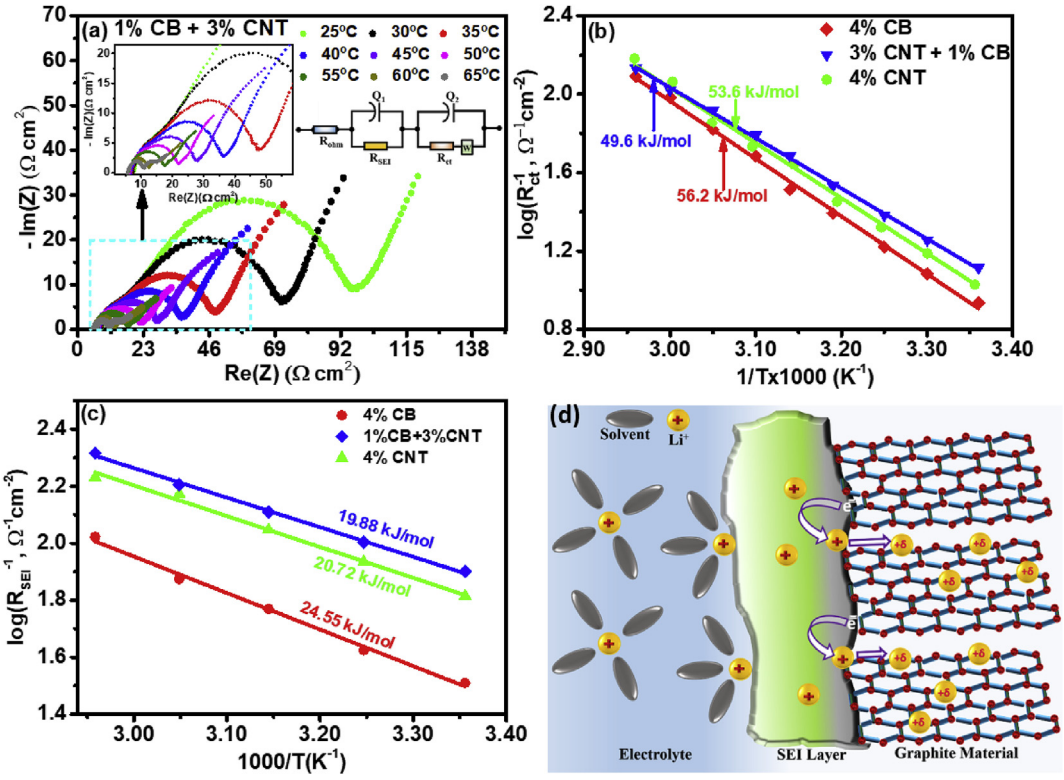

Fig. 6. (a) EIS spectra of MCMB electrode recorded at different temperatures with 1% CB and 3% CNT as conducting additives. Arrhenius behavior of inverse of resistance corresponding to charge-transfer (b) and migration through the SEI layer (c) are shown along with the corresponding activation energies computed using the slopes of these curves. (d) A schematic description of desolvation of solvated Li$^+$, electrochemical reaction and diffusion through SEI layer.

was thermally equilibrated for up to 3 h at the required temperature in the thermal chamber. The collected impedance data were fitted using the equivalent circuit shown in the inset Fig. 6(a) and the components related to kinetics, diffusion, and migration were deconvoluted.

As pointed out earlier, Li-ions from the solution combine with electrons to form metallic Li according to the electrochemical reaction $Li^{+}+e^{-} \rightleftarrows Li$ at the interface of solid and electrolyte phases. However, it has also been reported that Li exist in an ionic state in and out of graphitic material during intercalation/deintercalation process [60,61]. Li inside graphite layers polarizes owing to the significant difference in electronegativity of lithium and carbon, which have electronegativity values of 0.912 and 2.544, respectively. Subsequently, Li diffuses as Li-ion inside graphite layers. The polarization leads to a delocalization of electrons that depends on the nature of the conducting network in an electrode.

Typically, the EIS spectra for graphitic material in the intercalation voltage window consists of two depressed semicircles in high to medium frequencies and a sloping line in the low-frequency range. The depression in semicircles arises due to non-ideal capacitance behavior because of electrode surface roughness and porous microstructures [62,63]. In MCMB the high frequency (10^4–10^6 Hz) depressed semicircle is ascribed to lithium transfer through the solid electrolyte interface (SEI) film formed on the surface, while the medium frequency (10^2–10^4 Hz) semicircle is attributed to the interfacial electrochemical reaction and desolvation of solvated lithium ion. For illustration purpose, results shown in Fig. 6(a) clearly exhibit that the two depressed semicircles are well separated in the lower temperature range and hence the associated resistances (R_{SEI} and R_{ct}) from the impedance spectra can be accurately extracted. However, as the temperature increases, the two semicircles merge to suggest that processes occur at similar time scales at the higher temperature. The reciprocal of resistances associated with depressed semicircles, i.e., $1/R_{SEI}$ and $1/R_{ct}$, can be regarded as proportional to Li-ion transport conductivity through the SEI layer and interfacial Li-ion transfer, respectively. Assuming that both these processes are thermally activated such that the Arrhenius-type equation is valid, we write

$$\frac{1}{R_{ct}} = A_{ct} \exp\left(-\frac{E_{a.ct}}{RT}\right) \quad (4)$$

where the symbols A_{ct}, $E_{a.ct}$, R and T are frequency factor for charge transfer, charge transfer activation energy, universal gas constant and absolute temperature, respectively. A similar expression can be written for the conductivity of Li-ion through SEI layer. Hence, the activation energy can be extracted from the slope of the $\log(1/R_{ct})$ and $\log(1/R_{SEI})$ vs. 1/T plot.

Systematic measurements as described above were conducted with the MCMB electrodes containing 4 wt.% each of CB, CNT and hybrid 1%CB+3%CNT. As shown in Fig. 6(b) and c, in all cases a linear curve is observed to be an excellent fit for interfacial charge transport as well as transport through the SEI layer, demonstrating the applicability of the Arrhenius behavior. The extracted values of activation energy for various cases are shown in Fig. 6(b) and c and are also compared with those reported in the literature in Table 3.

These values of activation energy for transport of Li-ion through SEI and interfacial electrochemical reaction for electrodes containing different nano-fillers fall into two rather different ranges. The former lies within 20–25 kJ/mol while the latter in 50–60 kJ/mol. The schematic description of various steps of migration and reaction are shown in Fig. 6(d). Among them, the critical steps are stripping of solvation sheath at SEI layer, movement of ion through solid interface layer and the occurrence of the electrochemical reaction at the active surface before intercalation of lithium into the graphene layers. According to a previously stated argument [52,53], the first range is linked with a naked Li-ion intercalation; the second was suggested to correspond to the intercalation of solvated Li-ion that involves disintegration of the solvent sphere coordinated around Li-ion, also known as “solvation sheath”. The stripping-off of the coordinated solvent requires additional energy. However, the activation energy for charge transfer is not merely the result of desolvation of Li-ion, but surface chemistry also plays a crucial role in dictating the rate of interfacial charge transfer reaction [54].

It can be observed from Table 3 that MCMB electrode containing 4% CB as conducting additive displays a higher activation energy for migration through SEI and charge transfer compared with electrodes formed by replacing CB-filler with the same amount of CNT. This finding implies that the electrode exhibits an improved kinetics due to the reduction in the activation energy barrier for both interfacial charge transfer and migration through SEI layer. The high intrinsic electronic conductivity of CNT and the formation of a robust conducting network with interlaced nanotubes are obvious reasons for this improvement with CNT as an additive. In our earlier study, we suggested that the entire structure of conducting network remains intact even after continuous charging/discharging signifying a relatively stable conducting scaffold that results in a reasonably dense and quite stable surface layer on MCMB [21]. This aspect can now be quantified in terms of resistances corresponding to interfacial charge transfer and SEI migration as is done in Table 4.

Table 3
Activation energy for Li-ion migration through SEI layer, charge transfer reaction and solid-phase diffusion.

Nano-Fillers	$E_{a,SEI}$ (kJ/mol)		$E_{a,ct}$ (kJ/mol)		$E_{a,Diff}$ (kJ/mol)	
	This Work	Literature	This Work	Literature	This Work	Literature
CB	24.55	20.77 [58]	56.2	58.0 [56]	37.39	35.00 [64]
CNT	20.72		53.6	69.5 [58]	37.32	28.62 [65]
CB + CNT	19.88		49.6		37.84	36.23 [66]

Table 4
SEI layer and charge transfer resistances at different temperature for MCMB composite electrodes consisting different nano-fillers in at 0.16 V vs. Li/Li^{+}.

Nano-Fillers	CB		CNT		CB + CNT	
T(°C)	$R_{SEI}(m\Omega cm^2)$	$R_{ct}(m\Omega cm^2)$	$R_{SEI}(m\Omega cm^2)$	$R_{ct}(m\Omega cm^2)$	$R_{SEI}(m\Omega cm^2)$	$R_{ct}(m\Omega cm^2)$
25	30.92	116.29	15.32	84.55	12.57	76.67
35	23.73	60.15	11.63	51.17	9.91	41.35
45	17.01	30.7	8.98	22.79	7.77	20.68
55	13.35	15.13	6.71	14.025	6.22	12.14

The data presented shows a reduction in SEI layer resistance for CNT nano-fillers compared to CB. On the other hand, a mixture of CB and CNT in 1:3 wt proportion results in a further reduction in activation energy for movement of active species through surface layer and interfacial electrochemical reaction. The variation in activation energy in presence of different nano-fillers obtained in our work signifies that the surface layer formed with different conducting network changes the path for the interfacial electrochemical reaction. This, in turn, leads to an improved electrochemical reaction rate on the electrode surface resulting in the formation of a thin and stable SEI film.

On the basis of this discussion, it can be inferred that the charge transfer reaction is a result of a combination of desolvation of Li-ion, SEI chemistry, and concentration of free electron on the edge surface of graphite. The main steps for Li-ion intercalation into graphene plane are schematically described in Fig. 6(d). As shown, the solvated Li-ion in liquid electrolyte gets stripped-off from the solvent during migration through the SEI layer. After desolvation, the interfacial electrochemical reaction occurs that follows the formation of a graphitic intercalated compound (GIC). A partial exchange of electrons ($+\delta = 0.8e$ - $0.85e$ [60]) takes place between the graphene layers and lithium, generating highly mobile charge carriers in the graphite layers. This charge transfer exchange works as both the driving force for intercalation and the source of improvement of electrical conductivity of the host material.

3.4. Stage formation and transition

For a study of the solid-state kinetics of Li-ion in a graphitic carbon, it is essential to understand the resulting structural changes along with electrochemical behavior of Li-ion insertion-deinsertion process in such an electroactive material. Typical open circuit potential (OCP) curves of MCMB material are shown in Fig. 7. These OCP curves were obtained at 0.01C-rate in the voltage range of 0.005V–2.0 V vs. Li/Li^+ after performing the formation cycles at 27±1 °C. Several characteristic plateaus are observed during charge and discharge process which correspond to stage I – IV compounds [67]. The red circles on the voltage profile of Fig. 7 indicate the presence of single phase; as one stage grows at the expense of the other, the regions between consist of a two-phase zone. To draw a comparison among various phases, the plot of differential capacity against voltage is shown in the inset of Fig. 7. The peaks in differential capacity indicate the presence of two phases which can also be seen from XRD results shown in Fig. 8.

Three major and two minor couples of redox peaks can be observed from the differential plot in Fig. 7 at 0.202 V, 0.148 V, 0.125 V, 0.116 V and 0.083 V during insertion and 0.221 V, 0.194 V, 0.169 V, 0.129 V and 0.091 V during deinsertion. Two suppressed peaks detected during intercalation at a voltage of 0.148 V and 0.125 V are due to the presence of phases IV + III and III + IIL, respectively. Similarly, the peaks for these phases during deintercalation are observed at 0.194 V and 0.169 V. It is imperative to note that in earlier studies only three peaks were observed corresponding to the coexistence of stage I + II, II + III and IL + IV [68–70]. The schematic demonstration of Li-ion staging in graphitic material based on Daumas-Herold (D-H) model [71] is also shown in Fig. 7. According to this model, when Li-ion intercalates into graphite, a periodic arrangement of Li-ion species and graphene layers are formed. In a n-stage arrangement, a collection of Li-ions is separated by 'n' number of graphene layers. The Li-ions in one layer attract each other by elastic or strain mediated interaction. This attraction between Li-ions of one domain is highly attractive whereas the interaction between Li-ions of two different domains is slightly repulsive [72]. According to the model, Li-ions can move in between graphene layers whereas ion transport across the layer is not allowed [73]. As can be seen from the XRD spectra in Fig. 8, the major peaks at 2θ of 26.4°, 43.3° and 50.4° are attributed to the (002), (101) and (102) planes, respectively. During intercalation the average spacing between graphene layers increases which reflects as a shift in the XRD pattern corresponding to (002) plane only. The other dimensions of the graphite crystallite do not undergo appreciable change due to the Li-ion insertion process into the solid phase [67,70]. Hence, the peaks associated with (101) and (102) planes remain unaffected. Our results show that the average spacing between graphene layers increases gradually from 3.35 Å to 3.70 Å on lithiation which is in very good agreement with earlier results [68]. This expansion in the graphitic material has been considered to be a rather mild structural rearrangement by assuming the graphite layers as elastic plates [72,74]. Zabel et al. [75] has also reported that the graphene layers in graphite crystallite are flexible with a high value of stretch and shear interactions.

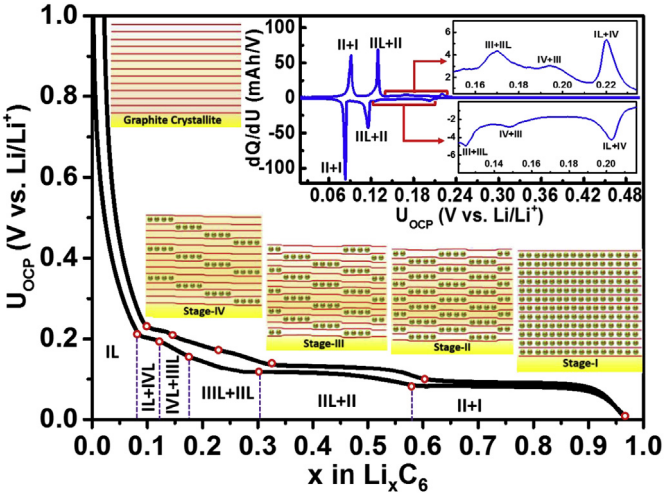

Fig. 7. Open circuit potential (OCP) of charge/discharge profile measured at C/100 rate with differential capacity plot to understand phase transformation with a schematic representation of Li^+ intercalation into graphite through different stages.

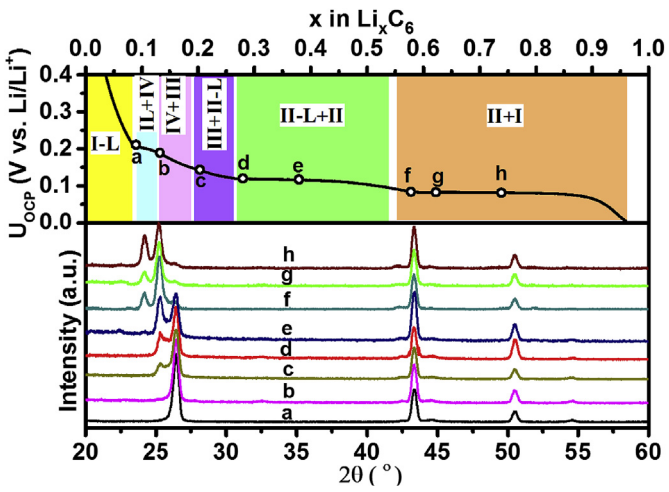

Fig. 8. XRD profiles measured after different stages of lithiation of MCMB electrode as marked in the OCP curve of Fig. 7 to illustrate the existence of different phases and variation of spacing between adjacent graphene layers in MCMB.

3.5. Solid-phase diffusion

Another crucial kinetic parameter that has relevance in deciding the performance of batteries especially at higher rates is solid-phase diffusivity of Li-ion into the graphitic material. The rate of electrochemical reaction at high rate intercalation/deintercalation process is dictated by diffusion due to the rather low diffusivity [41]. Several techniques including impedance spectroscopy [24–27], current electroanalytical methods such as potentiostatic intermittent titration technique (PITT) [23] and galvanostatic intermittent titration technique (GITT) [76,77] have been proposed to measure the diffusion coefficient in graphitic materials. The reported value of diffusivity of Li-ion in graphitic anode varies in the range from 10^{-7} to 10^{-15} cm^2/s [23–27,37,38,78]. This considerable variation in diffusivity with same technique is partially associated with uncertainty in the actual surface at which the electrochemical insertion/deinsertion takes place. In this work, GITT due to its superiority over other methods [76] has been applied to MCMB composite electrode containing different conducting nano-fillers. According to the analytical theory for GITT proposed by Weppner and Huggins [79], the Li-ion diffusion coefficient in solid-phase of the active material can be evaluated by using the following equation.

$$D^s_{GITT} = \left(\frac{2V_m}{M_w S_{ECAS}\sqrt{\pi\tau}}\right)^2 \left(\frac{\Delta E_s}{\Delta E_\tau}\right)^2 \quad (5)$$

When $\tau \ll R^2/D^s_{GITT}$. Here, V_m and M_w are the molar volume (cm^3/mol) and molecular weight (g/mol) of graphite compound, respectively, S_{ECAS} is the electrochemically active surface area per unit mass (cm^2/g) as calculated earlier, ΔE_s is the difference between steady-state potential before and after the current pulse, i.e., change in thermodynamic potential, and ΔE_τ is the change in potential during the current pulse (excluding *IR* effect) as demonstrated in the right panel of Fig. 9.

After completing cell formation cycles (i.e., five charging/discharging cycles at C/5 rate), the GITT experiment was conducted at room temperature for cells containing different types of nano-fillers (i.e., CB, CNT, and CB + CNT). During the GITT experiment, the cell was initially charged with a constant current pulse at C/20-rate for 15 min and then allowed to relax for 3 h in an open-circuit condition. The above procedure was repeated until the cell voltage reached a value of 0.01 V vs. Li/Li^+. For demonstration, the GITT curve as a function of the stoichiometric coefficient (x) is shown in Fig. 9 of MCMB electrode containing 1 and 3 wt. % of CB and CNT, respectively, as conducting additives. The estimated values of solid-state diffusion coefficient D^s_{GITT} from GITT curves for all cells with different conducting additives as a function of x is also shown in Fig. 9.

It can be observed from Fig. 9 that the diffusion coefficient displays a near identical behavior for all conducting nano-fillers. The results are also in good agreement with those available in the literature [37,79]. Moreover, a few remarkable observations regarding the variation of diffusion coefficient with stoichiometric coefficient in the solid-phase can be drawn.

As shown in Fig. 9, the solid-state diffusion coefficient exhibits two minima when plotted against Li-ion concentration in solid-phase. This is attributed to the coexistence of two-phase domains as was observed in the differential capacity plot as well as XRD analysis shown in Figs. 7 and 8, respectively. It can be observed from the XRD spectra in Fig. 8 that the peak at 26.4° which corresponds to average graphene layer interspace (i.e., d_{002} spacing) starts to gradually split into two peaks on Li-ion insertion in MCMB. The diffraction pattern recorded at voltages as marked on the OCP curve corresponding to d-h suggest that the d_{002} peaks migrate towards lower 2θ value with new peaks appearing and the intensity of original peaks diminishing. This infers the coexistence of two-phases in which the new phase starts forming at the expense of the existing phase.

In a two-phase system, the kinetics of intercalation process is derived from the strain-mediated interaction that does exist in mixed stage [80,81]. This attractive interaction between intercalated species during the transition stage in the lithium-graphite intercalated compound can be modeled assuming a Frumkin type isotherm with negative interaction coefficient [37] as

$$\frac{D}{D_0} = 1 + g[x(1-x)] \quad (6)$$

where D_0 is diffusion coefficient when there is no interaction between intercalated species (Langmuir isotherm), or in other words when $g = 0$. Since the two minima are observed in Fig. 9, two different values of the interaction coefficient corresponding to phases II-L + II and II + I namely, g_1 and g_2, respectively, are

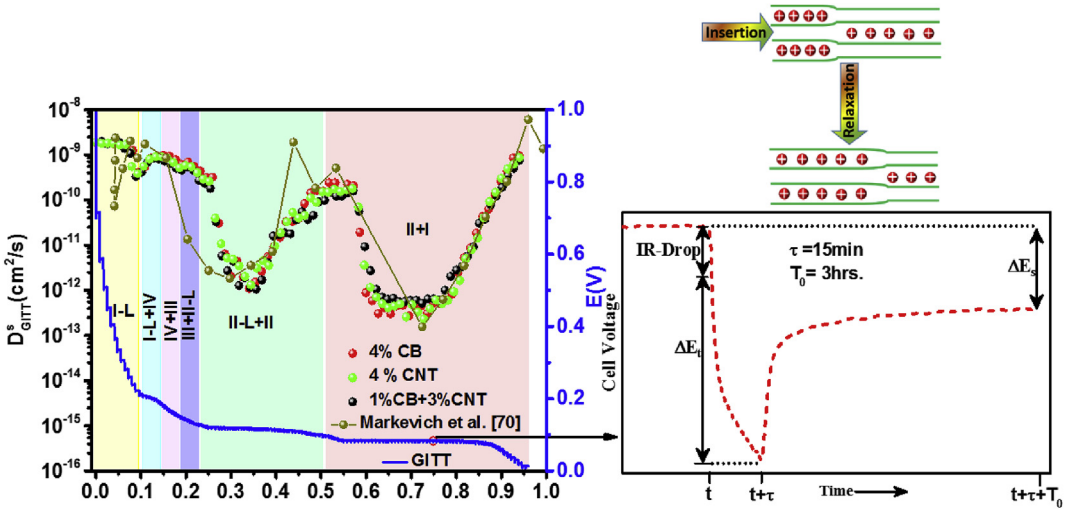

Fig. 9. GITT profile for MCMB electrode as a function of stoichiometry 'x' in the voltage range of 1.0 V - 0.005 V and corresponding Li^+ diffusion coefficient values for different conductive additives. A schematic for a single step of GITT experiment is also shown to demonstrate a potential response to the constant current pulse.

expected.

The diffusion process in solid-stage is considered as a series of elementary jumps along the potential energy surface and the activation energy (E_a) is termed as the rate of success for such leaps. Li-ion diffusion in graphite has been studied theoretically using the first-principle method in several papers [28,66,83,84]. Toyoura et al. [83] studied the diffusion of lithium in stage-I of a Li-graphite intercalated compound based on transition state theory and termed diffusion under lithium excess conditions due to an interstitialcy mechanism. The calculated activation energies for the diffusion coefficients under the lithium excess and deficient conditions were also different and given as 0.30 and 0.49 eV, respectively [83]. Persson et al. [28] reported that the energy barriers for Li-ion migration is 0.308 eV at x = 0.2 and 0.40 eV close to the ordered LiC_6 phase. Uthaisar et al. [66] observed that the diffusion process is quite fast near the edge, but it slows down as the Li-ion moves away from the surface and into the particle with the energy barrier calculated to be 0.376 eV [66]. These findings indicate that the lower energy barrier is expected to be localized to a few nanometers from the edges.

The Nyquist plots measured at different temperatures and as shown in Fig. 6(a) also provide a basis for determining the diffusivity in the solid. The solid-phase diffusion coefficient can be obtained from EIS spectra through the following equation [82]:

$$D^{s}_{EIS} = \left(\frac{V_m}{mS_{ECAS}F\sigma_w\sqrt{2}}\right)^2\left(\frac{\partial E}{\partial x}\right)^2 \quad (7)$$

Here m and V_m are the mass (g) and molar volume (cm^3/mol) of MCMB graphite material, respectively, F is the Faraday's constant, ϕ_w is the Warburg coefficient which is calculated from the slope of Re(Z) (or −Im(Z)) vs. $\frac{1}{\sqrt{\omega}}$ plot, and S_{ECAS} is the electrochemically active surface area per unit mass (cm^2/g). $\frac{\partial E}{\partial x}$ is the slope of electrode potential vs. composition x which can be calculated from the differential capacity plot as given in the inset of Fig. 7. The temperature dependence of the diffusion coefficient of Li-ion species between the layers of the graphitic crystallite of MCMB electrode containing different nano-fillers (CB, CNT, and CB + CNT) was measured using impedance spectroscopy. The diffusion coefficient was calculated using equation (7). The estimated values of diffusivity for all electrodes having different nano-fillers was fitted as a function of temperature according to Arrhenius type equation (8). The activation energy for the diffusion process can be estimated from the slope of these linear curves, with the estimated values shown in Table 5.

$$D_s = D_0 \exp\left[\frac{E_{a,D}}{R}\left(\frac{1}{T_0}-\frac{1}{T}\right)\right] \quad (8)$$

We compare the results of this study with those reported previously [64–66]. It is apparent that very few experimental studies have dealt with the determination of the activation energy for diffusion process in graphitic material. For example, the values for the activation energy for solid-phase diffusion have been reported as 35.0 kJ/mol [64] and 28.82 kJ/mol [65]. Clearly, these values are consistent with the activation energy calculated in our work.

Based on the estimated values, the diffusion process is postulated to be consisting of two elementary jumps that pass through an intermediate metastable state. This process is schematically explained by path-II in Fig. 10. Based on our experimental findings, where the activation barrier is calculated to be within 0.387–0.392 eV, it can be reasonably concluded that the more favorable mechanism for solid state diffusion of Li-ion in MCMB material at x = 0.2 is path-II as shown in Fig. 10.

Table 5
Activation energy for Li-ion solid-phase diffusion.

Nano-Fillers	$E_{a,Diff}$		
	Present study		Reported values (in kJ/mol)
	(in kJ/mol)	(in eV)	
CB	37.39	0.388	35.00 [64]
CNT	37.32	0.387	28.62 [65]
CB + CNT	37.84	0.392	36.23 [66]

4. Conclusions

In this work, a comparative study of detailed kinetic parameters on the role of conducting additives nano-fillers to the composite electrodes is performed. The influence of carbon black (CB), multi-walled carbon nanotubes (CNT), and hybrid (CB + CNT) conducting additives in MCMB electrode is investigated by means of physical, electrochemical, electroanalytical and crystallographic techniques with the aim of ascertaining the role of conducting nano-fillers in influencing the electrochemical reaction rate performance in carbon anode of Li-ion batteries. One possible factor that incorporates inconsistency among kinetic parameters is electrode surface area, therefore, to remove any discrepancy the electrochemically active

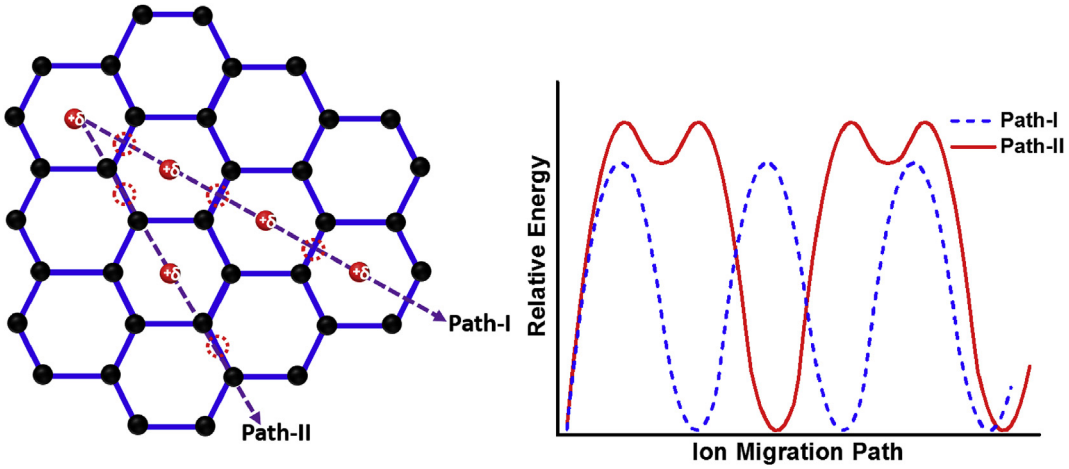

Fig. 10. Schematic of solid state diffusion mechanism in graphitic carbon.

surface area of the electrode was evaluated beforehand by image processing. A series of kinetic parameters were explored in a half-cell with MCMB carbon as a working electrode reinforced with different conducting nano-fillers (CB, CNT, and CB + CNT). It was found that at moderately high C-rate (2C < C-rate < 6C) the electrochemical reaction rate is controlled by interfacial kinetics. The electrode with hybrid CB + CNT nano-fillers offers better reaction kinetics parameters in contrast to CNT whereas in case of CB the performance is even poor. This is because, at high current loads, the rate determining step is the transport of active species (Li^+ and e^-) to the electrochemically active surface. Therefore, hybrid fillers which provide better short-range and long-range conducting pathways with sufficient contact with MCMB results in improved kinetic parameters in contrast to CNT where a well-dispersed CNT displays only long-range conducting electron pathway. Whereas in case of CB only short-range point-to-point contact results in the poor conducting network. Moreover, solid-phase diffusion of Li-ion remains essentially unaffected with different nano-fillers however, its display wavy-nature and this is attributed to the coexistence of two-phase domains in which the kinetics of intercalation process is derived from strain mediated interaction that does exist in the mixed stage. However, a completely ordered state is free of these strain and the kinetics is governed by a diffusion process. The stage formation was revealed through x-ray diffraction of cells at different SOC as well as differential capacity plot vs. voltage. The presence of peaks in differential plot and XRD peaks bifurcating suggests the presence of two-phase region.

To obtain further insight, the thermal study of transport and kinetic parameters of MCMB electrode with various nano-fillers is also analyzed. The Li-ion transfer at the interface of electrolyte and electrode, Li-ion migration through SEI layer formed on the surface of the active material and species transport in solid-phase was investigated by impedance spectroscopy at a different temperature. The resistance ascribe to each process was deconvoluted from impedance spectra and the corresponding Arrhenius plot was drawn for each case. It was observed that the activation energy for charge transfer reaction and activation energy for SEI layer diffusion are 56.2, 53.6, 49.6 kJ/mol and 24.55, 20.72 and 19.88 kJ/mol for CB, CNT and CB + CNT respectively which exhibit the ease of electron transfer for better conducting network and good ionically conducting SEI layer formation for improved electronically conducting network. The activation energy for solid phase diffusion was observed and it was found that it remains constant to around 0.39 eV for each case which implies that there is no discernible impact of conducting nano-fillers in species migration inside a solid phase. These estimated kinetic and transport parameters and there temperature dependence for different nano-fillers can reliably be used in thermal, electrochemical, or aging modeling of batteries involve MCMB carbon as anode material.

Acknowledgment

Financial support from Council of Scientific & Industrial Research (CSIR) under 22/648/13/EMR-II is gratefully acknowledged.

Appendix A. Supplementary data

Supplementary data to this article can be found online at https://doi.org/10.1016/j.electacta.2018.12.006.

References

[1] J.M. Tarascon, M. Armand, Issues and challenges facing rechargeable lithium batteries, Nature 414 (2001) 359.
[2] J.B. Goodenough, Y. Kim, Challenges for rechargeable Li batteries, Chem. Mater. 22 (2010) 587.
[3] M. Winter, J.O. Besengard, M.E. Spahr, P. Novak, Insertion electrode materials for rechargeable lithium batteries, Adv. Mater. 10 (1998) 725.
[4] W.A. Van Schalkwijk, B. Scrosati, Advances in Lithium-ion Batteries, Springer, New York, 2002.
[5] K. Tatsumi, N. Iwashita, H. Sakaebe, H. Shioyama, S. Higuchi, A. Mabuchi, H. Fujimoto, The influence of the graphitic structure on the electrochemical characteristics for the anode of secondary lithium batteries, J. Electrochem. Soc. 142 (1995) 716.
[6] A. Mabuchi, K. Tokumitsu, H. Fujimoto, T. Kasuh, Charge-discharge mechanism of graphitized mesocarbon microbeads, J. Electrochem. Soc. 142 (1995) 3049.
[7] K. Tatsumi, T. Akai, T. Imamura, K. Zaghib, N. Iwashita, S. Higuchi, Y. Sawada, ^{7}Li-nuclear magnetic resonance observation of lithium insertion into mesocarbon microbeads, J. Electrochem. Soc. 143 (1996) 1923.
[8] R. Alcantara, F.J.F. Madrigal, P. Lavela, J.L. Tirado, J.M.J. Mateos, C.G. de Salazar, R. Stoyanova, E. Zhecheva, Characterisation of mesocarbon microbeads (MCMB) as active electrode material in lithium and sodium cells, Carbon 38 (2000) 1031.
[9] W.J. Yuan, Y. Zhou, Y.R. Li, C. Li, H.L. Peng, J. Zhang, Z.F. Liu, L.M. Dai, G.Q. Shi, The edge- and basal-plane-specific electrochemistry of a single-layer graphene sheet, Sci. Rep. 3 (2013) 2248.
[10] S. Banerjee, J. Shim, J. Rivera, X. Jin, D. Estrada, V. Solovyeva, X. You, J. Pak, E. Pop, N. Aluru, R. Bashir, Electrochemistry at the edge of a single graphene layer in a nanopore, ACS Nano 7 (2012) 834.
[11] H. Li, H. Zhou, Enhancing the performances of Li-ion batteries by carbon-coating: present and future, Chem. Commun. 48 (2012) 1201.
[12] Q. Cheng, Porous graphene sponge additives for lithium ion batteries with excellent rate capability, Sci. Rep. 7 (2017) 925.
[13] M. Gaberscek, R. Dominko, J. Jamnik, Is small particle size more important than carbon coating? An example study on $LiFePO_4$ cathodes, Electrochem. Commun. 9 (2007) 2778.
[14] Y.D. Cho, G.T.K. Fey, H.M. Kao, The effect of carbon coating thickness on the capacity of $LiFePO_4$/C composite cathodes, J. Power Sources 189 (2009) 256.
[15] K.S. Chen, R. Xu, N.S. Luu, E.B. Secor, K. Hamamoto, Q. Li, S. Kim, V.K. Sangwan, I. Balla, L.M. Guiney, J.-W.T. Seo, X. Yu, W. Liu, J. Wu, C. Wolverton, V.P. Dravid, S.A. Barnett, J. Lu, K. Amine, M.C. Hersam, Comprehensive enhancement of nanostructured lithium-ion battery cathode materials via conformal graphene dispersion, Nano Lett. 17 (2017) 2539.
[16] X.F. Zhou, F. Wang, Y.M. Zhu, Z.P. Liu, Graphene modified $LiFePO_4$ cathode materials for high power lithium ion batteries, J. Mater. Chem. 21 (2011) 3353.
[17] S. Huang, Z. Wen, X. Zhu, Z. Lin, Effects of dopant on the electrochemical performance of $Li_4Ti_5O_{12}$ as electrode material for lithium ion batteries, J. Power Sources 165 (2007) 408.
[18] A.L.M. Reddy, A. Srivastava, S.R. Gowda, H. Gullapalli, M. Dubey, P.M. Ajayan, Synthesis of nitrogen-doped graphene films for lithium battery application, ACS Nano 4 (2010) 6337.
[19] F.C. Zheng, Y. Yang, Q.W. Chen, High lithium anodic performance of highly nitrogen-doped porous carbon prepared from a metal-organic framework, Nat. Commun. 5 (2014) 5261.
[20] F. Joho, B. Rykart, R. Imhof, P. Novak, M.E. Spahr, A. Monnier, Key factors for the cycling stability of graphite intercalation electrodes for lithium-ion batteries, J. Power Sources 81 (1999) 243.
[21] S. Ahamad, M. Ahmad, B.R. Mehta, A. Gupta, Effect of nano-fillers on capacity retention and rate capability of mesocarbon microbeads anode, J. Electrochem. Soc. 164 (2017) A2967.
[22] Z. Ogumi, M. Inaba, Electrochemical lithium intercalation within carbonaceous materials: intercalation processes, surface film formation, and lithium diffusion, Bull. Chem. Soc. Jpn. 71 (1998) 521.
[23] M.D. Levi, D. Aurbach, The mechanism of lithium intercalation in graphite film electrodes in aprotic media. Part 1. High resolution slow scan rate cyclic voltammetric studies and modelling, J. Electroanal. Chem. 421 (1997) 79.
[24] M. Umeda, K. Dokko, Y. Fujita, M. Mohamedi, I. Uchida, J.R. Selman, Electrochemical impedance study of Li-ion insertion into mesocarbon microbead single particle electrode. Part I. Graphitized carbon, Electrochim. Acta 47 (2001) 885.
[25] N. Takami, A. Satoh, M. Hara, T. Ohsaki, Structural and kinetic characterization of lithium intercalation into carbon anodes for secondary lithium batteries, J. Electrochem. Soc. 142 (1995) 371.
[26] P. Yu, B.N. Popov, J.A. Ritter, R.E. White, Determination of the lithium ion diffusion coefficient in graphite, J. Electrochem. Soc. 146 (1999) 8.
[27] J. Shim, K.A. Striebel, Electrochemical characterization of thermally oxidized natural graphite anodes in lithium ion batteries, J. Power Sources 164 (2007) 862.
[28] K. Persson, V.A. Sethuraman, L.J. Hardwick, Y. Hinuma, Y.S. Meng, A. van der Ven, V. Srinivasan, R. Kostecki, G. Ceder, Lithium diffusion in graphitic carbon, J. Phys. Chem. Lett. 1 (2010) 1176.
[29] T.R. Jow, M.B. Marx, J.L. Allen, Distinguishing Li+ charge transfer kinetics at NCA/electrolyte and graphite/electrolyte interfaces, and NCA/electrolyte and LFP/Electrolyte interfaces in Li-ion cells, J. Electrochem. Soc. 159 (2012) A604.
[30] A. Funabiki, Impedance study on the electrochemical lithium intercalation into natural graphite powder, J. Electrochem. Soc. 145 (1998) 172.
[31] O.S. Mendoza-Hernandez, H. Ishikawa, Y. Nishikawa, Y. Maruyama, Y. Sone, M. Umeda, State of charge dependency of graphitized-carbon-based reactions in a lithium-ion secondary cell studied by electrochemical impedance

spectroscopy, Electrochim. Acta 131 (2014) 168.
[32] M.C. Smart, B.V. Ratnakumar, Effects of electrolyte composition on lithium plating in lithium-ion cells, J. Electrochem. Soc. 158 (2011) A379.
[33] R.M. Wightman, M.R. Deakin, P.M. Kovach, W.G. Kuhr, K.J. Stutts, Methods to improve electrochemical reversibility at carbon electrodes, J. Electrochem. Soc. 131 (1984) 1578.
[34] M.T. McDermott, K. Kneten, R.L. McCreery, Anthraquinonedisulfonate adsorption, electron-transfer kinetics, and capacitance on ordered graphite electrodes: the important role of surface defects, J. Phys. Chem. 96 (1992) 3124.
[35] K.K. Cline, M.T. McDermott, R.L. McCreery, Anomalously slow electron transfer at ordered graphite electrodes: influence of electronic factors and reactive sites, J. Phys. Chem. 98 (1994) 5314.
[36] R.J. Rice, R.L. McCreery, Quantitative relationship between electron transfer rate and surface microstructure of laser-modified graphite electrodes, Anal. Chem. 61 (1989) 1637.
[37] M.D. Levi, D. Aurbach, Diffusion coefficients of lithium ions during intercalation into graphite derived from the simultaneous measurements and modeling of electrochemical impedance and potentiostatic intermittent titration characteristics of thin graphite electrodes, J. Phys. Chem. B 101 (1997) 4641.
[38] H. Yang, H.J. Bang, J. Prakash, Evaluation of electrochemical interface area and lithium diffusion coefficient for composite graphite anode, J. Electrochem. Soc. 151 (2004) A1247.
[39] T. Allen, Powder Sampling and Particle Size Determination, Elsevier, 2003.
[40] D. Lozano-Castello, D. Cazorla-Amoros, A. Linares-Solano, S. Shiraishi, H. Kurihara, A. Oya, Influence of pore structure and surface chemistry on electric double layer capacitance in non-aqueous electrolyte, Carbon 41 (2003) 1765.
[41] H. Buqa, D. Goers, M. Holzapfel, M.E. Spahr, P. Novak, High rate capability of graphite negative electrodes for lithium-ion batteries, J. Electrochem. Soc. 152 (2005) A474.
[42] A.J. Bard, L.R. Faulkner, Electrochemical Methods: Fundamentals and Applications, John Wiley & Sons, New York, 2001.
[43] J.O.M. Bokris, A.K.N. Reddy, M.E. Gamboa-Aldeco, Modern Electrochemistry 2A: Fundamentals of Electrodics, second ed., Kluwer Academic/Plenum Publishers, 2000.
[44] R.A. Marcus, On the theory of oxidation-reduction reaction involving electron transfer, J. Chem. Phys. 24 (1956) 966.
[45] R.A. Marcus, On the theory of electron-transfer reaction.VI. Unified treatment for homogeneous and electrode reactions, J. Chem. Phys. 43 (1964) 679.
[46] E. Laborda, M.C. Henstridge, A. Molina, F. Martínez-Ortiz, R.G. Compton, "A comparison of Marcus–Hush vs. Butler–Volmer electrode kinetics using potential pulse voltammetric techniques, J. Electroanal. Chem. 660 (2011) 169.
[47] S.-I. Cho, S.-G. Yoon, Characterization of $LiCoO_2$ thin film cathodes deposited by liquid-delivery metallorganic chemical vapor deposition for rechargeable lithium batteries, J. Electrochem. Soc. 149 (2002) A1584.
[48] P.J. Bouwman, B.A. Boukamp, H.J.M. Bouwmeester, P.H.L. Notten, Influence of diffusion plane orientation on electrochemical properties of thin film $LiCoO_2$ electrodes, J. Electrochem. Soc. 149 (2002) A699.
[49] K.A. Striebel, E. Sakai, E.J. Cairns, Impedance studies of the thin film $LiMn_2O_4$/electrolyte interface, J. Electrochem. Soc. 149 (2002) A61.
[50] K. Dokko, N. Nakata, Y. Suzuki, K. Kanamura, High-rate lithium deintercalation from lithiated graphite single-particle electrode, J. Phys. Chem. C 114 (2010) 8646.
[51] M. Ecker, T.K.D. Tran, P. Dechent, S. Kabitz, A. Warnecke, D.U. Sauer, Parameterization of a physico-chemical model of a lithium-ion battery: I. determination of parameters, J. Electrochem. Soc. 162 (2015) A1836.
[52] T. Abe, F. Sagane, M. Ohtsuka, Y. Iriyama, Z. Ogumi, Lithium-ion transfer at the interface between lithium-ion conductive ceramic electrolyte and liquid electrolyte-A key to enhancing the rate capability of lithium-ion batteries, J. Electrochem. Soc. 152 (2004) A2151.
[53] T. Abe, H. Fukuda, Y. Iriyama, Z. Ogumi, Solvated Li-ion transfer at interface between graphite and electrolyte, J. Electrochem. Soc. 151 (2004) A1120.
[54] K. Xu, "Charge-Transfer" Process at graphite/electrolyte interface and the solvation sheath structure of Li^+ in nonaqueous electrolytes, J. Electrochem. Soc. 154 (2007) A162.
[55] Y. Yamada, Y. Iriyama, T. Abe, Z. Ogumi, Kinetics of electrochemical insertion and extraction of lithium ion at SiO, J. Electrochem. Soc. 157 (2010) A26.
[56] Y. Yamada, Y. Iriyama, T. Abe, Z. Ogumi, Kinetics of lithium ion transfer at the interface between graphite and liquid electrolytes: effects of solvent and surface film, Langmuir 25 (2009) 12766.
[57] I. Skarmoutsos, V. Ponnuchamy, V. Vetere, S. Mossa, Li^+ solvation in pure, binary, and ternary mixtures of organic carbonate electrolytes, J. Phys. Chem. C 119 (2015) 4502.
[58] K. Xu, Y. Lam, S.S. Zhang, T.R. Jow, T.B. Curtis, Solvation sheath of Li^+ in nonaqueous electrolytes and its implication of graphite/electrolyte interface chemistry, J. Phys. Chem. C 111 (2007) 7411.
[59] Y. Yamada, K. Miyazaki, T. Abe, Role of edge orientation in kinetics of electrochemical intercalation of Lithium-ion of graphite, Langmuir 26 (2010) 14990.
[60] Y. Qi, H. Guo, L.G. Hector Jr., A. Timmons, Threefold increase in the Young's modulus of graphite negative electrode during lithium intercalation, J. Electrochem. Soc. 157 (2010) A558.
[61] C.T. Chan, W.A. Kamitakahara, K.M. Ho, P.C. Eklund, Charge-transfer effects in graphite intercalates: Ab initio calculations and neutron-diffraction experiment, Phys. Rev. Lett. 58 (1987) 1528.
[62] M.D. Levi, D. Aurbach, Simultaneous measurements and modeling of the electrochemical impedance and the cyclic voltammetric characteristics of graphite electrodes doped with lithium, J. Phys. Chem. B 101 (1997) 4630.
[63] D. Aurbach, B. Markovsky, I. Weissman, E. Levi, Y. Ein-Eli, On the correlation between surface chemistry and performance of graphite negative electrodes for Li ion batteries, Electrochim. Acta 45 (1999) 67.
[64] T.L. Kulova, A.M. Skundin, E.A. Nizhnikovskii, A.V. Fesenko, Temperature effect on the lithium diffusion rate in graphite, Russ. J. Electrochem. 42 (2006) 259.
[65] I. Umegaki, S. Kawauchi, H. Sawada, H. Nozaki, Y. Higuchi, K. Miwa, Y. Kondo, M. Mansson, M. Telling, F.C. Coomer, S.P. Cottrell, T. Sasaki, T. Kobayashi, J. Sugiyama, Li-ion diffusion in Li intercalated graphite C_6Li and $C_{12}Li$ probed by μ^+ SR, Phys. Chem. Chem. Phys. 19 (2017) 19058.
[66] C. Uthaisar, V. Barone, Edge Effects on the characteristics of Li diffusion in graphene, Nano Lett. 10 (2010) 2838.
[67] J.R. Dahn, Phase diagram of Li_xC_6, Phys. Rev. B 44 (1991) 9180.
[68] Z.X. Shu, R.S. McMillan, J.J. Murray, Electrochemical intercalation of lithium into graphite, J. Electrochem. Soc. 140 (1993) 922.
[69] T. Ohzuku, Y. Iwakoshi, K. Sawai, Formation of lithium-graphite intercalation compounds in nonaqueous electrolytes and their application as a negative electrode for a lithium ion (shuttlecock) cell, J. Electrochem. Soc. 140 (1993) 2490.
[70] J. Dahn, R. Fong, M. Spoon, Suppression of staging in lithium-intercalated carbon by disorder in the host, Phys. Rev. B 42 (1990) 6424.
[71] N. Daumas, A. Herold, Sur les relations entre la notion de atade et les mecanismes reactionnels dans les composes d'insertion du graphite. (On the relation between the stage structure and the reaction mechanism for graphite intercalation compounds), C. R. Acad. Sci. Paris 268 (1969) 373.
[72] G. Kirczenow, Interference phenomena in the theory of Daumas-Herold domain walls, Phys. Rev. Lett. 49 (1982) 1853.
[73] M.S. Dresselhaus, G. Dresselhaus, Intercalation compounds of graphite, Adv. Phys. 51 (2002) 1.
[74] V.A. Sethuraman, L.J. Hardwick, V. Srinivasan, R. Kostecki, Surface structural disordering in graphite upon lithium intercalation/deintercalation, J. Power Sources 195 (2010) 3655.
[75] H. Zabel, A. Magerl, J.J. Rush, Phonons in LiC_6, Phys. Rev. B 27 (1983) 3930.
[76] E. Markevich, M.D. Levi, D. Aurbach, Comparison between potentiostatic and galvanostatic intermittent titration techniques for determination of chemical diffusion coefficients in ion-insertion electrodes, J. Electroanal. Chem. 580 (2005) 231.
[77] D.W. Dees, S. Kawauchi, D.P. Abraham, J. Prakash, Analysis of the galvanostatic intermittent titration technique (GITT) as applied to a lithium-ion porous electrode, J. Power Sources 189 (2009) 263.
[78] M.D. Levi, E. Markevich, D. Aurbach, The effect of slow interfacial kinetics on the chronoamperometric response of composite lithiated graphite electrodes and on the calculation of the chemical diffusion coefficient of Li ions in graphite, J. Phys. Chem. B 109 (2005) 7420.
[79] W. Weppner, R.A. Huggins, Determination of the kinetic parameters of mixed-conducting electrodes and application to the system Li_3Sb, J. Electrochem. Soc. 124 (1977) 1569.
[80] S.A. Safaran, D.R. Hamann, Long-range elastic interactions and staging in graphite intercalation compounds, Phys. Rev. Lett. 42 (1979) 1410.
[81] Y. Zhu, C. Wang, Galvanostatic intermittent titration technique for phase-transformation electrodes, J. Phys. Chem. C 114 (2010) 2830.
[82] C. Ho, I.D. Raistrick, R.A. Huggins, Application of A-C techniques to the study of lithium diffusion in tungsten trioxide thin films, J. Electrochem. Soc. 127 (1980) 343.
[83] K. Toyoura, Y. Koyama, A. Kuwabara, I. Tanaka, Effects of off-stoichiometry of LiC_6 on the lithium diffusion mechanism and diffusivity by first principles calculations, J. Phys. Chem. C 114 (2010) 2375.
[84] E.M. Leggesse, C.-L. Chen, J.-C. Jiang, Lithium diffusion in graphene and graphite: effect of edge morphology, Carbon 103 (2016) 209.